



A low-crystalline ruthenium nano-layer supported on praseodymium oxide as an active catalyst for ammonia synthesis

Journal:	<i>Chemical Science</i>
Manuscript ID	SC-EDG-05-2016-002382.R2
Article Type:	Edge Article
Date Submitted by the Author:	25-Aug-2016
Complete List of Authors:	Sato, Katsutoshi; Kyoto University, Elements Strategy Initiative for Catalysts and Batteries Imamura, Kazuya; Oita University, Department of Applied Chemistry Kawano, Yukiko; Oita University, Department of Applied Chemistry Miyahara, Shin-ichiro; Oita University, Department of Applied Chemistry Yamamoto, Tomokazu; Kyushu University, Department of Applied Quantum Physics and Nuclear Engineering Matsumura, Syo; Kyushu University, Department of Applied Quantum Physics and Nuclear Engineering Nagaoka, Katsutoshi; Oita University, Department of Applied Chemistry

1 **A low-crystalline ruthenium nano-layer supported on**
2 **praseodymium oxide as an active catalyst for ammonia**
3 **synthesis**

4

5 Katsutoshi Sato,*^[a,b] Kazuya Imamura,^[b,+] Yukiko Kawano,^[b] Shin-ichiro Miyahara,^[a]

6 Tomokazu Yamamoto,^[c] Syo Matsumura,^[c] and Katsutoshi Nagaoka*^[b]

7

8 *[a] Elements Strategy Initiative for Catalysts and Batteries, Kyoto University. 1-30 Goryo-Ohara,*
9 *Nishikyo-ku, Kyoto 615-8245 (Japan)*

10 *[b] Department of Applied Chemistry, Faculty of Engineering, Oita University. 700 Dannoharu, Oita*
11 *870-1192 (Japan)*

12 *[c] Department of Applied Quantum Physics and Nuclear Engineering, Kyushu University. 744 Motooka,*
13 *Nishi-ku, Fukuoka 819-0395 (Japan)*

14 *[+] Present address: Research Laboratory of Hydrothermal Chemistry, Faculty of Science, Kochi*
15 *University. 2-5-1 Akebono-cho, Kochi 780-8520 (Japan)*

16

17 † Electronic supplementary information (ESI) available: Detailed procedures for each method,
18 catalytic performance, STEM-EDX images, detailed characterizations.

19

20 *Abstract*

21 **Ammonia is a crucial chemical feedstock for fertilizer production and is a potential energy**
22 **carrier. However, the current method of synthesizing ammonia, the Haber–Bosch process,**
23 **consumes a great deal of energy. To reduce energy consumption, a process and a**
24 **substance that can catalyze ammonia synthesis under mild conditions (low temperature**
25 **and low pressure) are strongly needed. Here we show that Ru/Pr₂O₃ without any dopant**
26 **catalyzes ammonia synthesis under mild conditions at 1.8 times the rates reported with**
27 **other highly active catalysts. Scanning transmission electron micrograph and energy**
28 **dispersive x-ray analyses revealed the formation of low-crystallite nano-layers of**
29 **ruthenium on the surface of the Pr₂O₃. Furthermore, CO₂ temperature-programmed**
30 **desorption revealed that the catalyst was strongly basic. These unique structural and**
31 **electronic characteristics are considered to synergistically accelerate the rate-determining**
32 **step of NH₃ synthesis, cleavage of the N≡N bond. We expect that use of this catalyst will**
33 **be a starting point for achieving efficient ammonia synthesis.**

34

35 ***Introduction***

36 Ammonia is one of the most important feedstocks in the modern chemical industry. Globally,
37 >80% of ammonia production is used to produce fertilizer, which is essential for growing crops.

38 ¹ In addition, ammonia has recently attracted attention as a carrier of energy and hydrogen.²⁻⁵

39 Ammonia is produced by combining atmospheric N₂ with hydrogen produced by renewable
40 energy. The ammonia is liquefied and transported to where it is used to generate power in
41 engines or electricity in fuel cells. Ammonia is being considered as a carrier of energy and
42 hydrogen because (1) it has a high energy density (12.8 GJ m⁻³) and (2) a high hydrogen content
43 (17.6 wt%), and (3) carbon dioxide is not released when hydrogen is produced by ammonia
44 decomposition.² If ammonia can be produced efficiently from renewable energy, it can
45 contribute to the solution of global problems related to energy and food production.

46 Currently, most ammonia is synthesized via the Haber–Bosch process.⁶⁻⁸ This process is a
47 major consumer of energy, accounting for about 1% of global energy consumption. In this
48 process, about 60% of consumed energy is recovered and saved to ammonia as enthalpy.
49 However, the remaining energy is lost, mainly during the production of hydrogen from natural
50 gas, ammonia synthesis, and gas separation. Because ammonia synthesis is carried out at very
51 high temperatures (>450 °C) and high pressures (>20 MPa), a major goal is reduction of the
52 high amount of energy used in this process.⁹ Curbing global energy consumption requires, inter

53 alia, a catalyst that is able to produce ammonia at much lower temperatures and pressures than
54 required for the iron-based catalysts used in the Haber–Bosch process.^{10–12}

55 Ruthenium is a possible catalyst for ammonia synthesis because of its higher activity at low
56 pressure and temperature than that of iron-based catalysts. The rate-determining step in NH₃
57 synthesis is cleavage of the N≡N bond of N₂, because the bond energy is very high (945 kJ mol⁻¹).^{13,14} It has been reported that modification of the morphology of the Ru surface (“structural
58 modification”) and of the Ru electronic states (“electronic modification”) are effective ways to
59 accelerate the rate-determining step and thus enhance the ammonia-synthesis activity of the Ru
60 catalyst.^{15,16} In the case of structural modification, the unusual unsaturated B₅-type site of Ru
61 has proven to be highly active.^{17–19} The B₅-type site consists of five Ru atoms: two at step edges
62 and three on the lower terrace. The five Ru atoms are all associated with the transition state of
63 adsorbed N₂, which results in weakening of the N≡N bond.¹⁷ Adjusting the Ru particle size (e.g.,
64 to 5 nm when the Ru particle is spherical) and changing the shape of Ru particles creates an
65 abundance of B₅-type sites.^{18,20,21} In the case of electronic modification, the use of basic supports
66 and the addition of a strong basic promoter to Ru catalysts have enhanced ammonia synthesis
67 activity dramatically.^{15,16} The mechanism involves transfer of electrons to the Ru metal from the
68 basic components. Transfer of electrons from Ru to the antibonding π -orbitals of N₂ then results
69 in weakening of the N≡N bond and promotion of N≡N cleavage.²² Weakening of the N≡N bond

71 by doping with strong basic oxides has been confirmed by observation of the N≡N stretching
72 frequency with infrared spectroscopy (IR); the most effective promoter has been reported to be
73 Cs₂O.^{23,24} In fact, most of the highly active Ru catalysts contain Cs₂O as a promoter.^{10,15,25,26}
74 However, CsOH, which may be produced in the presence of an H₂O impurity in the reactant,
75 has a low melting point (272 °C) and may move on the surface of the catalyst particles or
76 vaporize under the reaction conditions, the eventual result being degradation of the catalyst.²⁷
77 On the other hand, BaO is also reported as effective promoter and Ba-Ru/activated carbon
78 (Ba-Ru/AC) has been used in commercial industrial processes.²⁸ Recently, Horiuchi *et al.*
79 reported that Ru/BaTiO₃ and Ba-Ru/MgO show comparable high activity with Cs-Ru/MgO.²⁶
80 Notably, Ru-loaded electride [Ca₂₄Al₂₈O₆₄]⁴⁺(e⁻)₄ (Ru/C12A7:e⁻), which is a new class of Ru
81 catalyst supported on a non-oxide, shows high NH₃-synthesis activity without any dopant.^{10,29,30}
82 This high activity has been attributed to the high electron-donating power of the electride.

83 We show here that a praseodymium oxide-supported Ru catalyst (Ru/Pr₂O₃) without any
84 dopant exhibits unparalleled NH₃ synthesis ability compared with highly active catalysts
85 reported previously. The loading of Ru on the support was characterized by an unusual
86 morphology of low-crystallinity nano-layers, and the basicity of the catalyst was very high. We
87 show that the combination of these features facilitated the activation of N₂.

88

89 ***Results and discussion***90 **NH₃-synthesis activity and some properties over Ru/Pr₂O₃ catalysts**

91 Fig. 1 compares the NH₃-synthesis activity of the Ru/Pr₂O₃ with those of other supported Ru
92 catalysts under the same reaction conditions. Ba-Ru/activated carbon (Ba-Ru/AC) has been used
93 in industrial processes;²⁸ Cs-Ru/MgO is one of the most active Ru catalysts in NH₃ synthesis;
94 ^{25,31} and Ru/C12A7:e⁻ has attracted attention as a new active NH₃-synthesis catalyst.^{10–12} At
95 400 °C and 0.1 MPa (Fig. 1a), Ru/Pr₂O₃ and Cs-Ru/MgO gave NH₃ yields near thermodynamic
96 equilibrium (0.88%). Both the yields and NH₃ production rates were higher than those achieved
97 with Ru/C12A7:e⁻ and Ba-Ru/AC catalysts. In the industrial process, it is important to obtain
98 high one-pass NH₃ yields to avoid the high energy use required for gas separation. Furthermore,
99 from the standpoint of thermodynamic regulation, NH₃ synthesis is favored if the reaction is
100 carried out under high pressure.⁹ We therefore measured NH₃-synthesis activity at 1.0 MPa (Fig.
101 1b), where the NH₃ yield at thermodynamic equilibrium increases to 7.9%. Note that 1.0 MPa is
102 still much lower than the reaction pressure used for the Haber–Bosch process. With the increase
103 in reaction pressure, the differences in the activities of the catalysts were more pronounced: the
104 NH₃ yield reached 4.8% and the rate of formation obtained over Ru/Pr₂O₃ reached 19,000 μmol
105 h⁻¹ g⁻¹, >1.8 times the values associated with other catalysts.

106 To understand why rates of NH_3 synthesis are so high when catalyzed by $\text{Ru}/\text{Pr}_2\text{O}_3$, we
107 compared the characteristics of $\text{Ru}/\text{Pr}_2\text{O}_3$ with those of Ru/MgO and Ru/CeO_2 . All of the
108 catalysts were loaded with 5 wt% Ru. Among the dopant-free simple oxide-supported Ru
109 catalysts, Ru/MgO and Ru/CeO_2 have shown relatively high NH_3 -synthesis activity,³² and CeO_2
110 is a rare-earth oxide like Pr_2O_3 . Fig. S2 shows x-ray diffraction patterns of the catalysts after
111 activation in pure H_2 at 400 °C. In the cases of Ru/MgO and Ru/CeO_2 , only diffraction patterns
112 assigned to cubic-type MgO and CeO_2 were obtained. In the case of $\text{Ru}/\text{Pr}_2\text{O}_3$, the diffraction
113 peaks were attributed to rare earth C-type Pr_2O_3 .³³ On the other hand, that no diffraction peaks
114 of Ru species were apparent in the patterns of the catalyst samples suggests that crystallite size
115 of loaded Ru was too small to be detected. NH_3 -synthesis activities of the Ru catalysts were
116 then measured at 0.9 MPa after reduction at 400 °C. $\text{Ru}/\text{Pr}_2\text{O}_3$ catalyzed a much higher rate of
117 NH_3 synthesis than Ru/MgO and Ru/CeO_2 at all temperatures from 310 to 390 °C (Fig. 2). At
118 390 °C in particular, the NH_3 synthesis rate of $\text{Ru}/\text{Pr}_2\text{O}_3$ was 15,200 $\mu\text{mol g}^{-1} \text{h}^{-1}$, much higher
119 than those of Ru/CeO_2 (7,400 $\mu\text{mol g}^{-1} \text{h}^{-1}$) and Ru/MgO (1,500 $\mu\text{mol g}^{-1} \text{h}^{-1}$). Furthermore, the
120 long-term stability of the $\text{Ru}/\text{Pr}_2\text{O}_3$ catalyst at 390 °C under 0.9 MPa was evidenced by the fact
121 that the rate of NH_3 synthesis was stable for 50 h (Fig. S3).

122 Specific surface areas of $\text{Ru}/\text{Pr}_2\text{O}_3$, Ru/CeO_2 , and Ru/MgO were 20.4, 33.5, and 46.4
123 $\text{m}^2 \text{g}^{-1}$, respectively (Table 1). There was no clear correlation between specific surface area and

124 catalytic activity. Interestingly, the H/Ru ratio, a measure of Ru dispersion, was very low for
125 Ru/Pr₂O₃ compared with the other catalysts. As a result, the turnover frequency of Ru/Pr₂O₃ was
126 >3.5 times that of Ru/CeO₂ and Ru/MgO. These results suggest that the high turnover frequency
127 of Ru/Pr₂O₃ makes possible the excellent rate of synthesis of NH₃ (activity per weight of
128 catalyst).

129

130 **Structural properties of Ru/Pr₂O₃**

131 As the NH₃-synthesis ability of a supported Ru catalyst is related to the morphology of the
132 loaded Ru and the basicity of the support material, we used scanning transmission electron
133 micrograph (STEM) observations and energy dispersive x-ray (EDX) analyses to investigate the
134 morphology. Figs. 3 and S4 show high-angle annular dark-field (HAADF) images and EDX
135 maps of Ru/Pr₂O₃ following treatment of the catalyst with H₂ at 400 °C. Figs. S5 and S6 show
136 analogous images and maps of Ru/CeO₂ and Ru/MgO, respectively. A number of particles
137 identified as Ru species by EDX were supported on MgO and CeO₂, but were seldom observed
138 over Pr₂O₃. However, the EDX map showed that Ru was dispersed over the entire Pr₂O₃ surface.
139 In the reconstructed overlapping EDX images, the greenish edges of the catalyst particles
140 indicated that the surfaces of the catalyst particles were covered by Ru species. These results
141 suggest that the state of Ru is completely different when it is loaded over Pr₂O₃ versus MgO and

142 CeO₂. To further investigate the surface morphology, we made high-resolution STEM
143 (HR-STEM) observations (Fig. 4, and see Figs. S7–9). On Ru/MgO and Ru/CeO₂, the lattice
144 fringes of the Ru species and supports were clearly apparent. The d space of the Ru species was
145 0.21 nm, which is consistent with that of the (101) plane of metallic Ru. Mean diameters of the
146 Ru particles were 1.8 ± 0.7 nm on Ru/MgO and 2.5 ± 0.8 nm on Ru/CeO₂. In addition, the
147 surface of the support of these catalysts was smooth, and changes in the lattice fringe were
148 clearly observed on the boundaries between Ru particles and supports (Figs. 4b, 4c, S8, and S9).
149 In contrast, on Ru/Pr₂O₃, the surface of the Pr₂O₃ was covered by layers of Ru rather than by
150 particles. That lattice fringes of most parts of the Ru layers were not apparent indicated that
151 crystallinity of the Ru layers was low. The thickness of the Ru layers was 0.5–3 nm, and Ru
152 particles were sometimes included in the layers. Thus, we considered that the surface of the
153 Pr₂O₃ was covered mainly with low-crystalline Ru nano-layers.

154 To explain why the Ru on the Pr₂O₃ support possessed such a unique morphology, we
155 measured x-ray diffraction patterns of the catalyst precursors of Ru/Pr₂O₃. As shown in Fig. S10,
156 the bare support [before impregnation with Ru₃(CO)₁₂] showed the structure of fluorite-type
157 Pr₆O₁₁. However, after impregnation with Ru₃(CO)₁₂ in tetrahydrofuran (THF) and drying, the
158 peaks assigned to Pr₆O₁₁ became smaller, and peaks attributed to Pr(OH)₃ and PrOOH appeared
159 instead. Furthermore, after heat treatment under a stream of Ar at 350 °C, only PrOOH was

160 observed. At this point, the HAADF STEM and overlay of the EDX maps of the Ru/Pr₂O₃
161 demonstrated that the surfaces of the catalyst particles were covered by Ru species (Fig. S11).
162 These results indicate that Ru₃(CO)₁₂ reacted with the O²⁻ in Pr₆O₁₁. Pr⁴⁺ was reduced to Pr³⁺
163 with the formation of CO₂. The support then reacted with the H₂O impurity in the THF, and
164 after heat treatment in the Ar stream, Ru and PrOOH were formed. In brief, the results reveal
165 that the high reactivity between Ru₃(CO)₁₂ and Pr₆O₁₁ prevented aggregation of Ru₃(CO)₁₂ with
166 Ru₃(CO)₁₂ and contributed to formation of the unique structure of the loaded Ru. The rough
167 surface of the Pr₂O₃ and fuzziness of the boundary between Ru and Pr₂O₃ in the HR-STEM
168 image in Fig. 4a and S7 was probably due to the reaction between Ru₃(CO)₁₂ and Pr₆O₁₁.
169 Furthermore, during H₂ treatment, PrOOH was converted to Pr₂O₃ (Figs. S2). During this
170 process, part of the Ru included in the Ru layers was crystalized to Ru particles, and thus Ru
171 particles were sometimes observed in the Ru layers in HR-STEM (Fig. S7). As shown in the
172 HR-STEM images, the Ru species over Pr₂O₃ were arranged in a low-crystalline, nano-layered
173 structure. In such a structure, unsaturated Ru atoms were not precisely arranged and formed
174 step-and-terrace sites similar to a B₅-type site. The unique surface morphology of Ru in
175 Ru/Pr₂O₃ would promote N₂ adsorption and subsequent cleavage of the N≡N bond.

176 In addition, we carried out STEM-EDX observations of Ru/Pr₂O₃ after the long-term
177 stability test shown in Fig. S3. As shown in Figs. S12 and S13, the Pr₂O₃ was still covered with

178 low-crystalline Ru nano-layers, as it was before reaction, and distinct changes of structure were
179 not observable. These results demonstrate the high durability of the unique surface structure of
180 Ru/Pr₂O₃ under the conditions used for NH₃ synthesis.

181

182 **Basic properties of Ru/Pr₂O₃**

183 We used CO₂ temperature-programmed desorption (CO₂-TPD) measurements of the catalysts
184 (Fig. 5) to evaluate another crucial determinant of NH₃-synthesis ability, the basicity of the
185 support. To remove the contribution of the CO₂ that remained on the surface even after H₂
186 reduction, we subtracted the CO₂-TPD profile without CO₂ adsorption from that after CO₂
187 adsorption (see Fig. S14 for original figures). CO₂ desorption was observed at 50–680 °C on
188 Ru/Pr₂O₃, 50–600 °C on Ru/CeO₂, and 50–500 °C on Ru/MgO. CO₂ desorption observed at
189 high temperature region (≥ 300 °C) was greatest on Ru/Pr₂O₃, intermediate on Ru/CeO₂, and
190 least on Ru/MgO. These results indicate that the basic sites on Ru/Pr₂O₃ are the strongest, and
191 those on Ru/MgO are the weakest. We used the total amount of CO₂ desorbed as a metric of
192 basic density over the catalysts. Ru/Pr₂O₃ had the highest basic density, 4.4 $\mu\text{mol m}^{-2}$, almost
193 twice those of Ru/CeO₂, 2.3 $\mu\text{mol m}^{-2}$, and Ru/MgO, 2.2 $\mu\text{mol m}^{-2}$. These results reveal that the
194 surface basicity of Ru/Pr₂O₃ was much stronger than those of Ru/MgO and Ru/CeO₂. This
195 strong surface basicity results in the most effective electron donation to Ru and promotes N₂

196 adsorption and subsequent cleavage of the $\text{N}\equiv\text{N}$ bond. Furthermore, we can say that Pr_2O_3 is
197 covered by islands of Ru nano-layers, which allow large amounts of CO_2 to adsorb on the
198 surface of uncovered Pr_2O_3 . Note also that the CO_2 desorption temperature and total density of
199 basic sites were higher on Ru/ CeO_2 than on Ru/MgO. This difference accounts for the higher
200 NH_3 -synthesis activity of Ru/ CeO_2 than of Ru/MgO.

201

202 **Activation of N_2 over Ru/ Pr_2O_3**

203 Finally, to understand the activation of N_2 molecules over the Ru/ Pr_2O_3 catalyst, we examined
204 the states of the adsorbed N_2 with FT-IR techniques. The IR spectra after the addition of N_2 to
205 Ru/MgO, Ru/ CeO_2 , and Ru/ Pr_2O_3 at room temperature are shown in Fig. 6. Each catalyst
206 showed broad peaks around 2350 to 2100 cm^{-1} ; such peaks are assignable to the stretching
207 vibration mode of the N_2 adsorbed with an end-on orientation to the Ru surface.^{21,23,24} Note that
208 the peak absorbance of N_2 adsorbed on Ru/ Pr_2O_3 occurred at a lower frequency (2178 cm^{-1})
209 than the corresponding peak absorbances on Ru/MgO (2210 cm^{-1}) and Ru/ CeO_2 (2189 cm^{-1}). In
210 the spectrum of $^{15}\text{N}_2$ adsorbed on Ru/ Pr_2O_3 , the peak absorbance was shifted to a lower
211 frequency (2104 cm^{-1}) than on Ru/ Pr_2O_3 (2178 cm^{-1}), is in good agreement with the frequency
212 estimated from the isotope effect ($2178 \text{ cm}^{-1} \times (14/15)^{1/2} = 2104 \text{ cm}^{-1}$).^{23,24} These results suggest
213 that these peaks are associated with N_2 on the Ru surfaces. The lower frequencies of the peak

214 absorbances of N_2 adsorbed on Ru/ Pr_2O_3 than on Ru/MgO and Ru/ CeO_2 indicate that the $N\equiv N$
215 bond of N_2 was further weakened over the low-crystalline Ru nano-layers on Pr_2O_3 relative to
216 Ru nanoparticles on the other supports. We surmise that the morphology of the Ru surface and
217 the basicity of the catalyst contributed synergistically to weakening the $N\equiv N$ bond and
218 enhancing the catalytic activity for NH_3 synthesis.

219

220 **Conclusions**

221 In summary, we demonstrated that Ru/ Pr_2O_3 without any dopant catalyzed a high rate of NH_3
222 synthesis under mild reaction conditions (0.1–1.0 MPa). Characteristics of the Ru/ Pr_2O_3 include
223 low-crystalline Ru nano-layers formed by the reaction between $Ru_3(CO)_{12}$ and Pr_6O_{11} and strong
224 basicity of the Pr_2O_3 . These characteristics are considered to synergistically accelerate the
225 rate-determining step of ammonia synthesis, cleavage of the $N\equiv N$ bond of N_2 . In addition,
226 substitution of a part of praseodymium with other element without degrading its activity for
227 NH_3 synthesis is currently in progress, because it is a kind of expensive elements. The research
228 outcome will appear in coming contribution. We believe that our catalyst will facilitate the
229 development of an effective method for synthesizing ammonia from renewable energy under
230 environmentally benign conditions. Such a method can be expected to contribute to the solution
231 of food and energy crises globally.

232 Acknowledgements

233 This work was supported by CREST, Japan Agency of Science and Technology (JST).
234 STEM/TEM observations were performed as part of a program conducted by the Advanced
235 Characterization Nanotechnology Platform Japan, sponsored by the Ministry of Education,
236 Culture, Sports, Science and Technology (MEXT), Japan. K. Sato thanks the Program for
237 Elements Strategy Initiative for Catalysts & Batteries (ESICB) commissioned by MEXT.
238 STEM/TEM observations with T. Toriyama (Kyushu University) is acknowledged. The authors
239 thank Mr. Y. Wada, Ms. M. K. Nakao, and Mr. T. Terasawa (Oita University) for assistance
240 with sample preparation, catalytic activity tests, and characterization techniques. We
241 acknowledge Prof. K. Shimizu (Hokkaido University) for fruitful discussions concerning IR
242 analysis.

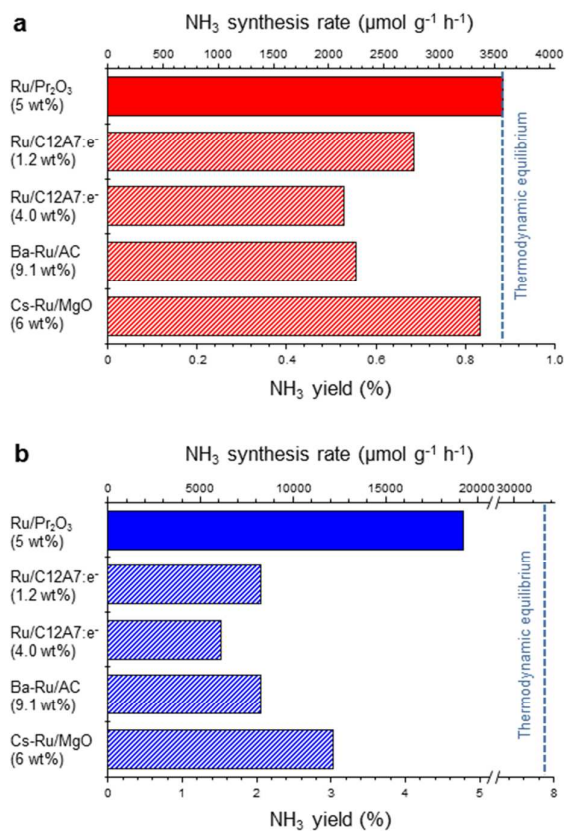
243

244 Notes and references

- 245 1. J. W. Erisman, M. A. Sutton, J. Galloway, Z. Klimont and W. Winiwarter, *Nat. Geosci.*,
246 2008, **1**, 636-639.
- 247 2. A. Klerke, C. H. Christensen, J. K. Nørskov and T. Vegge, *J. Mater. Chem.*, 2008, **18**,
248 2304-2310.
- 249 3. R. Schlögl, *ChemSusChem*, 2010, **3**, 209-222.
- 250 4. F. Schüth, R. Palkovits, R. Schlögl and D. S. Su, *Energy Environ. Sci.*, 2012, **5**,

- 251 6278-6289.
- 252 5. J. W. Makepeace, T. J. Wood, H. M. A. Hunter, M. O. Jones and W. I. F. David, *Chem.*
253 *Sci.*, 2015, **6**, 3805-3815.
- 254 6. H. Bielawa, O. Hinrichsen, A. Birkner and M. Muhler, *Angew. Chem. Int. Ed.*, 2001, **40**,
255 1061-1063.
- 256 7. T. Kandemir, M. E. Schuster, A. Senyshyn, M. Behrens and R. Schlogl, *Angew. Chem.*
257 *Int. Ed.*, 2013, **52**, 12723-12726.
- 258 8. S. Perathoner and G. Centi, *ChemSusChem*, 2014, **7**, 1274-1282.
- 259 9. C. W. Hooper, in *Catalytic Ammonia Synthesis, Fundamentals and Practice*, ed. J. R.
260 Jennings, Springer, US, 1991, Ammonia Synthesis: Commercial Practice, 253 - 283.
- 261 10. M. Kitano, Y. Inoue, Y. Yamazaki, F. Hayashi, S. Kanbara, S. Matsuishi, T. Yokoyama,
262 S. W. Kim, M. Hara and H. Hosono, *Nat. Chem.*, 2012, **4**, 934-940.
- 263 11. F. Hayashi, M. Kitano, T. Yokoyama, M. Hara and H. Hosono, *ChemCatChem*, 2014, **6**,
264 1317-1323.
- 265 12. Y. Inoue, M. Kitano, S.-W. Kim, T. Yokoyama, M. Hara and H. Hosono, *ACS Catal.*,
266 2014, **4**, 674-680.
- 267 13. S. Gambarotta and J. Scott, *Angew. Chem. Int. Ed.*, 2004, **43**, 5298-5308.
- 268 14. H. K. Chae, D. Y. Siberio-Perez, J. Kim, Y. Go, M. Eddaoudi, A. J. Matzger, M.
269 O'Keeffe and O. M. Yaghi, *Nature*, 2004, **427**, 523-527.
- 270 15. K. Aika, H. Hori and A. Ozaki, *J. Catal.*, 1972, **27**, 424-431.
- 271 16. K. Aika, M. Kumasaka, T. Oma, O. Kato, H. Matsuda, N. Watanabe, K. Yamazaki, A.
272 Ozaki and T. Onishi, *Appl. Catal.*, 1986, **28**, 57-68.
- 273 17. S. Dahl, A. Logadottir, R. C. Egeberg, J. H. Larsen, I. Chorkendorff, E. Törnqvist and J.
274 K. Nørskov, *Phys. Rev. Lett.*, 1999, **83**, 1814-1817.

- 275 18. C. J. H. Jacobsen, S. Dahl, P. L. Hansen, E. Törnqvist, L. Jensen, H. Topsøe, D. V. Prip,
276 P. B. Møenshaug and I. Chorkendorff, *J. Mol. Catal. A: Chem.*, 2000, **163**, 19-26.
- 277 19. S. Dahl, E. Tornqvist and I. Chorkendorff, *J. Catal.*, 2000, **192**, 381-390.
- 278 20. Z. Song, T. Cai, J. C. Hanson, J. A. Rodriguez and J. Hrbek, *J. Am. Chem. Soc.*, 2004,
279 **126**, 8576-8584.
- 280 21. Z. You, K. Inazu, K. Aika and T. Baba, *J. Catal.*, 2007, **251**, 321-331.
- 281 22. K. Aika, A. Ohya, A. Ozaki, Y. Inoue and I. Yasumori, *J. Catal.*, 1985, **92**, 305-311.
- 282 23. J. Kubota and K. Aika, *J. Chem. Soc., Chem. Commun.*, **1991**, 1544.
- 283 24. J. Kubota and K. Aika, *The Journal of Physical Chemistry*, 1994, **98**, 11293-11300.
- 284 25. K. Aika, T. Takano and S. Murata, *J. Catal.*, 1992, **136**, 126-140.
- 285 26. Y. Horiuchi, G. Kamei, M. Saito and M. Matsuoka, *Chem. Lett.*, 2013, **42**, 1282-1284.
- 286 27. J. G. van Ommen, W. J. Bolink, J. Prasad and P. Mars, *J. Catal.*, 1975, 38, **120**-127.
- 287 28. D. E. Brown, T. Edmonds, R. W. Joyner, J. J. McCarroll and S. R. Tennison, *Catal.*
288 *Lett.*, 2014, **144**, 545-552.
- 289 29. M. Kitano, Y. Inoue, H. Ishikawa, K. Yamagata, T. Nakao, T. Tada, S. Matsuishi, T.
290 Yokoyama, M. Hara and H. Hosono, *Chem. Sci.*, 2016, 7, 4036-4043.
- 291 30. Y. Lu, Li, T. Tada, Y. Toda, S. Ueda, T. Yokoyama, M. Kitano and H. Hosono, *J. Am.*
292 *Chem. Soc.*, 2016, **138**, 3970-3973.
- 293 31. F. Rosowski, A. Hornung, O. Hinrichsen, D. Herein, M. Muhler and G. Ertl, *Appl.*
294 *Catal., A*, 1997, **151**, 443-460.
- 295 32. Y. Niwa and K.-i. Aika, *Chem. Lett.*, 1996, 3-4.
- 296 33. G. Adachi and N. Imanaka, *Chem. Rev.*, 1998, **98**, 1479-1514.
- 297

298 **Figure 1**

299

300

301 **Fig. 1** Catalytic performance of supported Ru catalysts for NH₃ synthesis at (a) 0.1 MPa and (b)

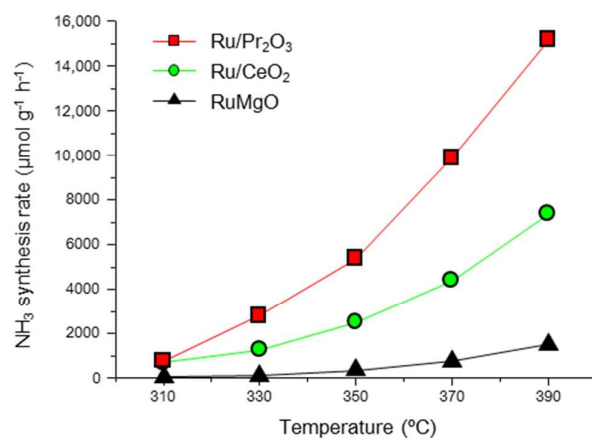
302 1 MPa. Reaction conditions: catalyst, 0.2 g; reactant gas, H₂/N₂ = 3 with a flow rate of 60 mL

303 min⁻¹; reaction temperature, 400 °C. With the exception of Ru/Pr₂O₃, NH₃ synthesis rates are

304 reproduced from Ref. [10].

305

306 **Figure 2**



307

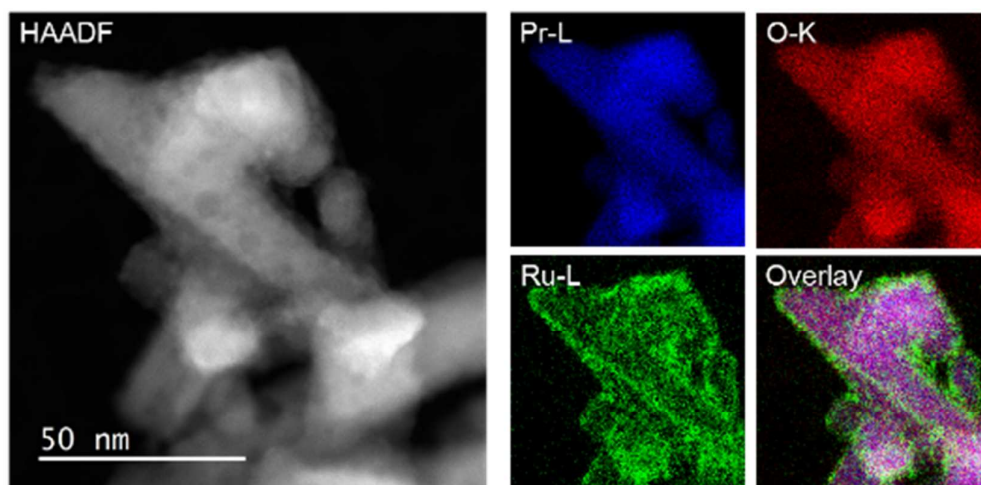
308

309 **Fig. 2** Rate of NH₃ synthesis over supported Ru catalysts. Reaction conditions: catalyst, 0.2 g;

310 reactant gas, H₂/N₂ = 3 with a flow rate of 60 mL min⁻¹; pressure, 0.9 MPa.

311

312 Figure 3



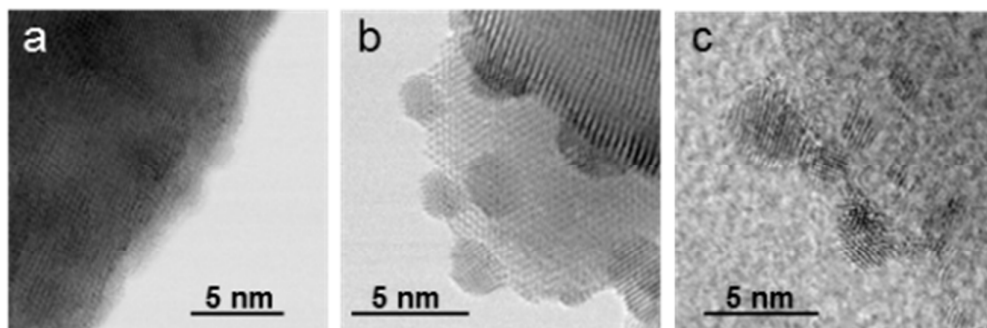
313

314

315 **Fig. 3** HAADF-STEM image, Pr-L, O-K, and Ru-L STEM-EDX maps, and reconstructed316 overlay image of Pr, O, and Ru for Ru/Pr₂O₃ after H₂ reduction.

317

318 Figure 4



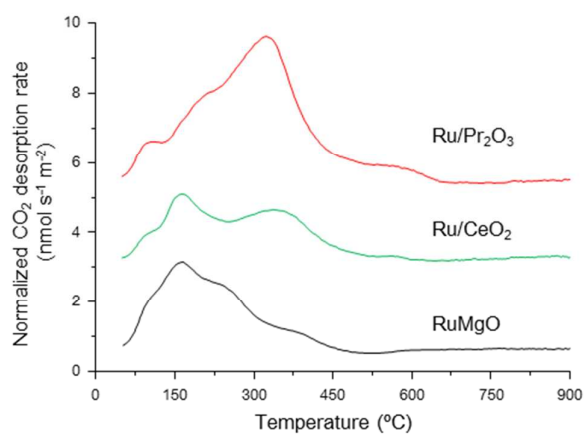
319

320

321 **Fig. 4** HR-STEM images of (a) Ru/Pr₂O₃, (b) Ru/CeO₂, and (c) Ru/MgO after H₂ reduction.

322

323 Figure 5



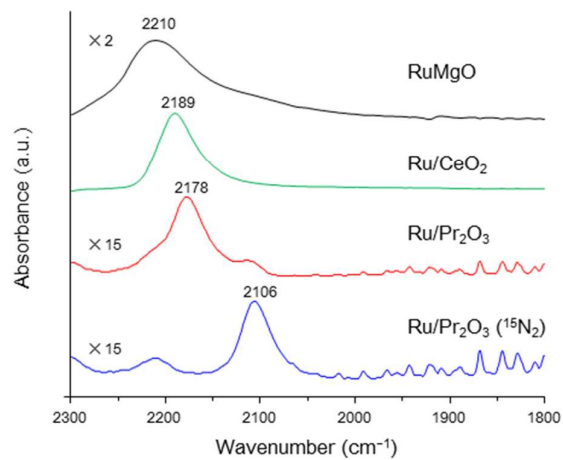
324

325

326 **Fig. 5** CO₂-TPD profiles of supported Ru catalysts. Following H₂ reduction at 400 °C, CO₂
327 adsorption was carried out at 50 °C. These curves show the difference between curves shown in
328 Fig. S14 to remove the contribution of CO₂ that remained on the surface of the catalyst even
329 after H₂ pre-treatment.

330

331 Figure 6



332

333

334 **Fig. 6** Difference infrared spectra of N₂ molecules before and after N₂ adsorption on supported

335 Ru catalysts. Spectra were collected under 6 kPa of N₂ (¹⁵N₂ for Ru/Pr₂O₃) at 25 °C.

336

337 Table 1

338 **Table 1.** Physicochemical properties of supported Ru catalysts.

Catalyst	Specific surface area ^[a] (m ² g ⁻¹)	H/Ru	Turnover frequency ^[b] (s ⁻¹)	Density of base sites ^[c] (μmol m ⁻²)
Ru/Pr ₂ O ₃	20.4	0.17	0.050	4.4
Ru/CeO ₂	33.5	0.29	0.014	2.3
Ru/MgO	46.4	0.3	0.003	2.2

339 [a] Estimated by using H₂ chemisorption capacity. [b] Calculated by using H/Ru value and NH₃ yield at
340 390 °C under 0.9 MPa. [c] Estimated by using CO₂-TPD.

341

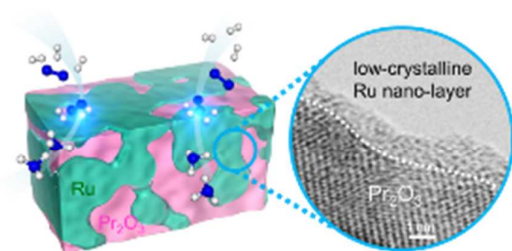
342 **Table of contents (Maximum 20 words)**

343

344 Low-crystalline Ru nano-layers and strong basicity of Ru/Pr₂O₃ synergistically accelerated the
345 rate-determining step of ammonia synthesis.

346

347



348